Preparation of Fly Ash Nickel Catalyst and its Application in Catalytic Pyrolysis of Rice Straw for Syngas Production

Kui Lan, Shuang Shang, Chaoqiang Guo, Tao Xiong, Zhenhua Qin, Weitao He, and Jianfen Li *

The catalytic pyrolysis of rice straw for syngas (H_2 + CO) production with nickel oxide (NiO)/fly ash catalysts was investigated in a horizontal fixed-bed quartz tube reactor. Besides, X-ray diffraction, X-ray fluorescence, field emission scanning electron microscopy, and Brunauer-Emmett-Teller analysis were employed to study the physiochemical properties of the catalysts before and after catalytic pyrolysis of biomass. The results illustrated that NiO was uniformly loaded on the surface of fly ash *via* a filament-like coating. Furthermore, the effects of calcination temperature (400 to 700 °C), reaction temperature (550 to 800 °C), holding time (5 to 35 min), and NiO loading (5 to 30 wt%) on the catalyst performance were investigated. Analysis of the gas composition showed that the NiO/fly ash catalyst had the best ability to increase H_2 and CO concentration at a 400 °C calcination temperature, 600 °C reaction temperature, 20 wt% NiO loading, and 20 min holding time. Compared with rice straw pyrolysis alone at these conditions, the concentration of H_2 and CO experienced a steep increase from 7 vol% to 41 vol% and 18 vol% to 34 vol%, respectively. The catalyst developed in this research opens a new pathway for the utilization of fly ash in the field of biomass pyrolysis.

Keywords: Fly ash; Catalytic pyrolysis; Rice straw; Syngas

*Contact information: School of Chemical and Environmental Engineering, Wuhan Polytechnic University, Wuhan 430023, China; *Corresponding author: lijfen@163.com*

INTRODUCTION

Renewable energy is gradually substituting for fossil fuels due to increasing energy demand worldwide (Yang *et al.* 2017). Biomass, water, solar, wind, and ocean energy accounts for approximately 14% of the world's energy demand (Panwar *et al.* 2011). Among renewable energy sources, biomass energy from agriculture, forests, and urban solid waste is one of the most promising sources of alternative energy due to its extensive sources, as well as its neutral property in CO_2 circulation (Field *et al.* 2008). China is a large agricultural country with a wide range of agricultural waste sources and high yields. In terms of crops, according to the data of the National Bureau of Statistics (2017), China's grain output reached $6.17*10^4$ million tons in 2017, of which the output of rice, maize, and wheat were $2.1*10^4$ million tons, $2.2*10^4$ million tons, and $1.3*10^4$ million tons, respectively. Therefore, it can be inferred that the crop straw resources in China are also abundant.

Pyrolysis is a thermochemical conversion technology for the efficient utilization of crop straw. It can convert low-value straw into high-quality syngas that can be used for power generation (Xue *et al.* 2017). During the biomass pyrolysis process, the generation of tar in gas product is one of the major issues, which is known for energy waste, blockage

of pipelines, and even as a threat to human health (Guo *et al.* 2018). Therefore, catalytic pyrolysis technology came into being. Compared with traditional non-catalytic pyrolysis, the use of catalysts in the pyrolysis process can reduce energy input, time, and cost, and improve the quality of syngas (Balasundram *et al.* 2018). Furthermore, catalytic pyrolysis can save the cost of tar removal in downstream processes. Thus, in recent years, there has been increasing interest in catalytic pyrolysis of biomass (Loy *et al*. 2018a). To date, a variety of catalysts, such as natural minerals, such as olivine (Michel *et al.* 2013) and dolomite (Yu *et al.* 2009), zeolites (Shao *et al.* 2018), alkali metals (Suzuki *et al.* 1992), noble metals (Furusawa and Tsutsumi 2005), non-nickel transition metals (Li *et al.* 2013; Duman *et al.* 2014), and nickel-based catalysts (He *et al.* 2009), have been extensively studied for syngas production in biomass pyrolysis. Noble metal catalysts have excellent catalytic performance, but they tend to be expensive (Akubo *et al.* 2018). Nickel-based catalysts are the most widely used among these catalysts due to their good activity/cost ratios (Świerczyński *et al.* 2007; Zhang *et al.* 2018). In general, natural minerals (dolomite, olivine) (Chang *et al.* 2014; Wang *et al.* 2017), zeolites (Buchireddy *et al.* 2010), and metal oxides (MgO, CaO, and Al_2O_3) (Choudhary and Mamman 2000; Li *et al.* 2010; Garbarino *et al.* 2015) are used as a catalyst's support. However, these supports are comparatively expensive. The cost of catalysts has always restricted its wide industrial application in biomass pyrolysis. Therefore, it is necessary to develop low-cost catalysts for the catalytic pyrolysis of straw in syngas production.

Fly ash (FA) is the main industrial solid waste discharged from coal-fired power plants. The output is huge, and the material is available at low cost. China's output of fly ash is approximately 500 to 700 million tons per year (Liu *et al.* 2018). The recycling of fly ash can maximize its value and reduce harm to the environment. At present, fly ash is widely used in the construction industry (Nagrockiene and Rutkauskas 2019; Wang and Zhao 2019), but only a few studies have been conducted on biomass catalytic pyrolysis. Li *et al.* (2006) mixed fly ash, red mud, and sodium bicarbonate at a mass ratio of 9.5:90:0.5 and calcined the mixture at 1090 °C to prepare a catalyst carrier for biomass pyrolysis. The results of characterization showed that the performance of the catalyst carrier was in accordance with industrial requirements. Loy *et al.* (2018b) used FA as the catalyst to produce syngas *via* catalytic pyrolysis of rice husk. The experimental results indicated that after using FA, the concentration of syngas reached 68.3 vol%. Compared with non-catalytic pyrolysis, the concentration of H_2 was increased by 8.4 vol%. The FA is mainly composed of SiO_2, Al_2O_3, Fe_2O_3, and CaO, with a large specific surface area and good adsorption performance, which makes it possible to be used as the catalyst carrier of rice straw catalytic pyrolysis. Because of the large use of catalysts during continuous operation, it is not feasible to use expensive catalysts. Hence, there is high novelty in the study of low-cost NiO/FA catalyst for catalytic pyrolysis of rice straw to produce syngas.

It is noteworthy that NiO can react with H_2 and CO in crude gas to be transformed into Ni, which can eliminate the step of activating the catalyst and simplify the process. Thus, NiO/FA was directly used for catalytic pyrolysis in the following experiment. In this paper, NiO/FA catalysts were made by the homogeneous precipitation method using FA as carrier. The catalytic effects of the NiO/FA catalysts on the syngas (H_2 + CO) production from rice straw were studied using a horizontal fixed-bed quartz tube reactor. In addition, the effects of operating conditions, such as calcination temperature, reaction temperature, holding time, and NiO loading, on syngas production were investigated to further examine the feasibility of FA as a nickel-based catalyst carrier.

EXPERIMENTAL

Materials

Rice straw (RS), collected in Wuhan, Hubei province, China, was chosen as the biomass feed stock in this study. Prior to testing, the rice straw was crushed and sieved to obtain particles in the size range of 0.5 mm to 1 mm. To eliminate the effect of moisture content, sufficient amounts of the rice straw samples were oven-dried at 105 °C for 24 h and then sealed in a desiccator to prevent absorption of moisture from the air. The ultimate and proximate analyses of the rice straw samples shown in Table 1 were conducted using an elemental analyzer (Flash 2000; Thermo Fisher Scientific, Waltham, MA, USA) and according to GB/T 28731 (2012), respectively. The fly ash was obtained from Zhengzhou in the Henan province of China with density of 2.4 kg/m^3. Before the experiments, it was also oven-dried at 105 °C for several hours. The X-ray fluorescence analysis (EDX-7000; Shimadzu, Kyoto, Japan) was used for examination of the chemical compositions of the fly ash as shown in Table 2.

Table 1. Proximate and Ultimate Analyses of the Rice Straw

Materials	Ultimate Analysis (wt%)						Proximate Analysis (wt%)			
	C	H	O*	N	S		M	A	V	FC
Rice straw	40.85	5.58	53.47	0.08	<0.01		9.3	8.4	77.82	4.48
* by difference; M: Moisture; V: Volatile matter; A: Ash; FC: Fixed Carbon										

Catalysts preparation

The catalysts were prepared through the homogeneous precipitation method using nickel nitrate hexahydrate ($Ni(NO_3)_2 \cdot 6H_2O$) and carbamide ($CO(NH_2)_2$), that were purchased from Aladdin Industrial Corporation (Shanghai, China). First, 10 g of dried FA was poured into a 500-mL round-bottom flask. Then, $Ni(NO_3)_2 \cdot 6H_2O$ and $CO(NH_2)_2$ with a mass ratio of 1:4 was mixed with 150 mL of deionized water. After the mixture had completely dissolved, the mixed solution was poured into the round-bottom flask and then stirred for 2 h in a 115 °C oil bath. The resulting mixture was filtered and dried at 105 °C for approximately 12 h. The dried catalyst precursor was calcined at different temperatures (400 °C, 500 °C, 600 °C, and 700 °C) with the heating rate of 10 °C /min for 2 h in an air atmosphere. Subsequently, the catalysts were obtained and defined as NiO/FA. According to the above method, NiO/FA catalysts with different NiO loadings (5 wt%, 10 wt%, 15 wt%, 20 wt%, 25 wt%, and 30 wt%) and different calcination temperatures were prepared.

Apparatus and Procedure

The laboratory-scale catalytic pyrolysis experimental set-up of the process, including the gas supply system, pyrolysis reactor, gas purification system, syngas collection, and analysis system, is depicted as a schematic diagram in Fig. 1. The tests were conducted in a horizontal fixed-bed quartz tube reactor on which the furnace could be slid. The reactor had an inner diameter of approximately 60 mm, was 1400 mm in total length, and 600 mm in the flat-temperature zone. Two quartz boats were used to hold the biomass samples and the catalyst, one boat for each. The boat had an inner diameter of 40 mm, length of 100 mm, and was 10 mm in height. The gas purification system consisted of one bottle of isopropanol, water, and silica gel (from left to right) and was immersed in an ice-water bath.

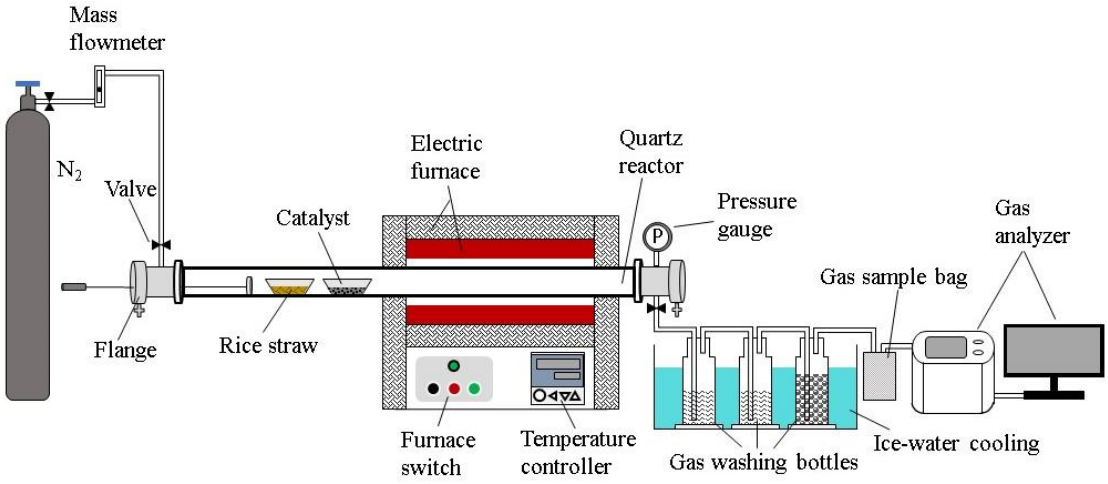

Fig. 1. Schematic diagram of the experimental system

First, 0.5 g NiO/FA catalyst and 1 g RS were loaded into two quartz boats in the reactor, and then the flanges on both sides were closed. A flow rate of 200 mL/min of nitrogen was continuously introduced into the entire system for 20 min under room temperature to supply an inert atmosphere throughout the reactor. Subsequently, the reactor was heated from normal to target temperature at a heating rate of 10 °C/min and kept constant for 20 min (holding time). When the flat-temperature zone was preheated to the target temperature, the two boats were quickly pushed to the furnace. After 20 min, the furnace was pushed away and the valves on both sides of the tube were opened. Meanwhile, the syngas was carried to a gas sample bag by the nitrogen gas. Finally, gas composition and content were determined using a gas analyzer. Each test was repeated three times to ensure the reliability of the data collected.

Methods

The crystal phases of the fresh and used catalysts were detected using an X-ray diffractometer (XRD-7000; Shimadzu, Kyoto, Japan). The morphological characteristics of FA and NiO/FA catalysts were elucidated from the images obtained using the field emission scanning electron microscope (JSM-7100F; JEOL, Ltd., Akishima, Japan). The coke deposit content of the used catalysts was examined *via* an elemental analyzer (Flash 2000; Thermo Fisher Scientific, Waltham, MA, USA). The textural properties of FA and NiO/FA catalysts were investigated using the N_2 adsorption–desorption measurements at 77 K (ASAP 2460; Micromeritics, Atlanta, GA, USA). It should be noted that all characterized catalysts were calcined at 400 °C with a NiO loading of 20 wt% unless otherwise stated. The volatile gas was collected with a gas sample bag and analyzed using an infrared gas analyzer (Gasboard-3100; Cubic-Ruiyi, Wuhan, China). Only the syngas (H_2 + CO) was measured in this study to evaluate the performance of the catalyst, considering that the contents of CH_4 and other hydrocarbons (C_nH_m) were negligible in comparison to other components.

RESULTS AND DISCUSSION

Characterization of NiO/FA Catalyst

X-ray fluorescence (XRF) analysis

The elemental compositions of FA and NiO/FA catalysts are shown in Table 2. The XRF spectrum showed high contents of SiO_2 and Al_2O_3 in the NiO/FA catalyst. In addition, different species of alkali metal oxides (*e.g.*, CaO, K_2O, and TiO_2) and transition metal oxides (*e.g.*, Fe_2O_3) were also detected, indicating that NiO/FA consisted of diverse chemical components. The content of NiO in the NiO/FA catalyst was 22.8%, which was higher than the theoretical loading of 20%. This may have been because XRF analysis is mainly for the micro-areas of the catalyst surface and is considered a semi-quantitative analysis (Bo *et al.* 2008), which led to some errors.

Table 2. XRF Analyses of the Fly Ash and NiO/FA Catalyst

Sample	Elemental Composition (wt%)							
	NiO	SiO_2	Al_2O_3	CaO	Fe_2O_3	K_2O	SO_3	TiO_2
FA	-	55.69	29.7	5.81	3.86	2.13	1.47	1.03
NiO/FA	22.8	46.91	19.44	3.57	3.53	2.01	0.46	1.05

X-ray diffraction (XRD) analysis

Figure 2 shows the XRD spectra of the FA and NiO/FA catalysts. There were some characteristic peaks at 2θ values of 16.4°, 26.3°, 31.0°, 33.2°, 35.3°, 40.9°, 42.6°, 53.9°, and 60.7°, from which the material can be identified as Mullite syn ($Al_6Si_2O_{13}$) based on the XRD pattern of the FA. Moreover, the characteristic peaks at 2θ values of 20.8°, 26.6°, and 50.0° corresponded to quartz (SiO_2). Furthermore, the crystalline phases at 2θ values of 33.2°, 39.3°, and 54.2° corresponded to haematite (Fe_2O_3). Meanwhile, it can be observed from the XRD pattern of the NiO/FA catalysts that the catalyst exhibited five distinguished peaks from 2θ values of 37.2° to 79.5° that indicate the presence of NiO. Therefore, it was concluded that Ni exited in the form of NiO and coincided with the XRF analysis.

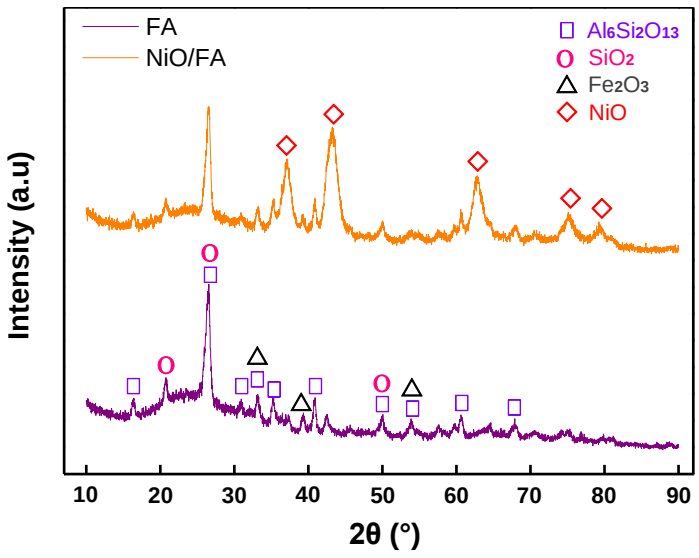

Fig. 2. XRD patterns of FA and NiO/FA catalysts

Field emission scanning electron microscopy (FESEM) analysis

The surface morphology of the FA and NiO/FA catalyst are presented in Fig. 3. Figure 3(a) shows that FA was composed of spherical beads with different sizes and regular shapes. From the image in Fig. 3(b), it can be observed that after loading with NiO, the surface of FA exhibited the morphological features of being coated with a rough film. In addition, the catalyst structure was relatively complete, and it basically kept the same regular shape as the carrier and without breakage after loading with NiO, indicating that the load effect was outstanding. Figure 3(c) shows that the NiO on the surface of FA was filament-wound and relatively fluffy. It was inferred that NiO uniformly covered the surface of FA and the catalyst provided more contact sites for tar-cracking in gas.

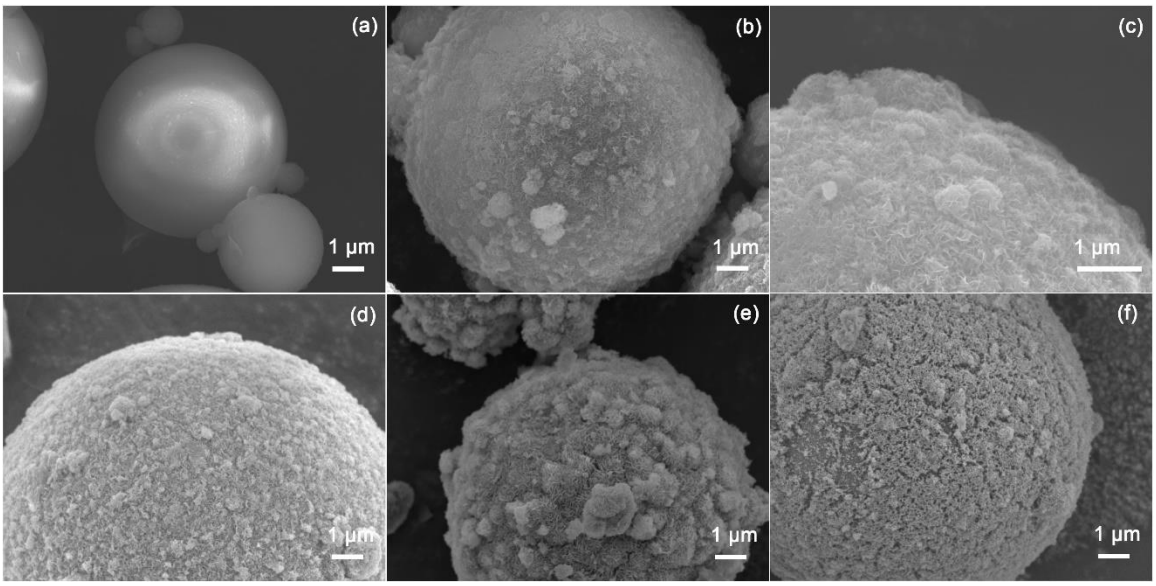

Fig. 3. FESEM images of (a) FA, (b) and (c) 20 wt% NiO/FA, (d) 10 wt% NiO/FA, (e) 30 wt% NiO/FA, and (f) used NiO/FA

Brunauer–Emmett–Taylor (BET) analysis

The textural properties of the carrier, fresh catalyst, and used catalyst are listed in Table 3. According to Table 3, the BET surface area of the fresh catalyst (31.9 $m^2 \cdot g^{-1}$) was much larger than that of the carrier, which was 0.56 $m^2 \cdot g^{-1}$. A higher BET surface area of the catalyst meant that there were more active sites on the surface for catalytic pyrolysis reaction to occur. Moreover, the total pore volume increased from 0.0015 $cm^3 \cdot g^{-1}$ to 0.115 $cm^3 \cdot g^{-1}$. This may have occurred because the filamentary NiO interlaced on the surface of FA and then formed a complex mesh structure, which greatly increased the BET surface area and total pore volume. The results were consistent with the FESEM analysis results. Furthermore, after the catalytic pyrolysis reaction, the BET surface area and total pore volume of NiO/FA decreased and the average pore diameter increased, mainly due to the coke deposition on the catalyst. Figure 3 (f) clearly shows that a layer of covering appeared on the surface of the used catalyst. And it can be seen from Table 4 that the coke deposition content of the used catalyst was 2.12 wt% at 600 °C reaction temperature. For both the fresh and used catalyst, the pore diameter was in the mesoporous range, which indicated that the catalyst was beneficial to the diffusion of gas molecules.

Table 3. Textural Properties of Carrier, Fresh, and Used Catalyst

Textural Properties	FA	Fresh NiO/FA	Used NiO/FA
BET surface area ($m^2 \cdot g^{-1}$)	0.56	31.9	9.79
Total pore volume ($cm^3 \cdot g^{-1}$)	0.0015	0.115	0.058
Average pore diameter (nm)	29.86	12.37	22.99

Catalytic Performance of NiO/FA Catalyst

Effect of calcination temperature

The effect of calcination temperature in the range of 400 °C to 700 °C on the concentration of H_2 and CO was investigated, while the reaction temperature, holding time, and NiO loading were fixed at 600 °C, 20 min, and 20 wt%, respectively. Figure 4 shows the concentration of H_2 and CO as a function of the calcination temperature of the NiO/FA catalyst. Figure 4 illustrates that when calcined at 400 °C, the activity of the catalyst was the highest, and the H_2 and CO concentration peaked at 41 vol% and 34 vol%, respectively. With the increase of calcination temperature from 400 °C to 700 °C, the concentration of syngas gradually decreased from 75 vol% to 58 vol%, which indicated that the catalytic activity of the catalyst receded several degrees.

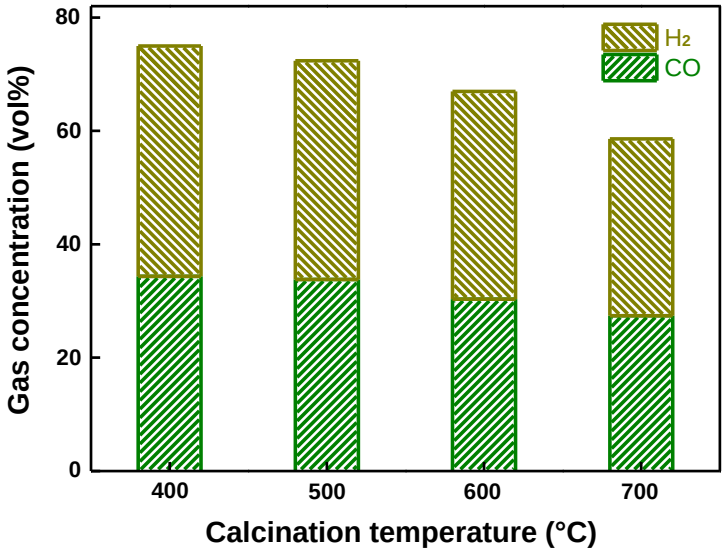

Fig. 4. Effect of calcination temperature on the concentration of H_2 (vol%) and CO (vol%)

Figure 5 shows XRD patterns of the NiO/FA catalyst (20 wt% of NiO loading) at different calcination temperatures. The active components of the catalysts exhibited characteristic diffraction peaks of NiO. Therefore, the phase of the active components was not changed by the different calcination temperatures. However, increased calcination temperature led to an increased intensity of the characteristic diffraction peaks of NiO. Furthermore, the shape of characteristic peaks became sharper and the half-peak width narrowed, revealing that the particle size of NiO in the catalyst gradually increased. In addition, the BET surface area of the catalysts decreased with the increase of calcination temperature, which were 31.9 $m^2 \cdot g^{-1}$ (400 °C), 21.85 $m^2 \cdot g^{-1}$ (500 °C), 18.62 $m^2 \cdot g^{-1}$ (600 °C), and 11.09 $m^2 \cdot g^{-1}$ (700 °C), respectively. These results meant that a higher metal dispersion probably took place at 400 °C. Similar results have been reported by Valle *et al.*

(2014), who reported the catalysts that are calcined at a lower temperature have a lower value of average NiO particle size and do well in dispersing metal. Consequently, in terms of this study, a lower calcination temperature corresponded with better catalytic activity of the catalyst. Other researchers have observed similar results. Gao *et al.* (2017) showed that the yields of H_2 and gas decreased from 85.79 g•kg^{-1} to 52.58 g•kg^{-1} biomass pyrolysis oil and 1.43 m^3•kg^{-1} to 1.02 m^3•kg^{-1} biomass pyrolysis oil, respectively, with the increase of calcination temperature from 400 °C to 700 °C. Courson *et al.* (2002) reported that the catalytic activity of Ni/olivine catalysts declined with increasing calcination temperatures in dry reforming of methane. A higher calcination temperature affected the particle size and dispersion degree of the active component (Roh *et al.* 2011). For this reason, 400 °C was the optimum calcination temperature for the NiO/FA catalyst in this study.

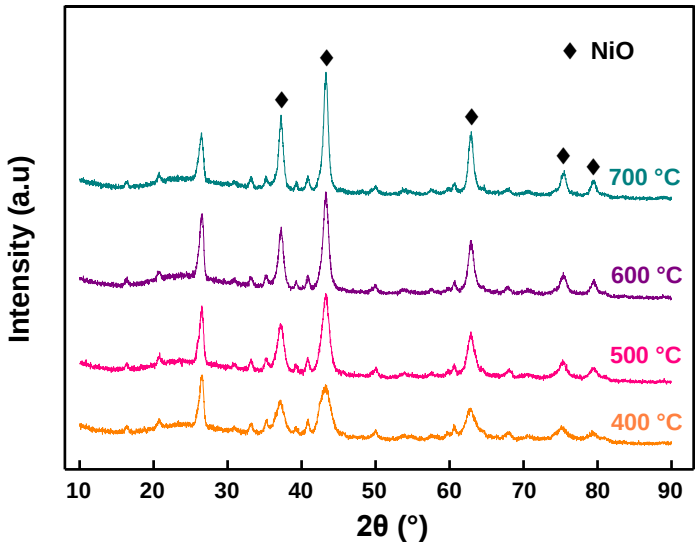

Fig. 5. XRD patterns of the NiO/FA catalysts with different calcination temperature

Effect of reaction temperature

The reaction temperature is one of the most crucial parameters influencing the concentration of biomass pyrolysis syngas (Sun *et al.* 2016). The effect of reaction temperature in the range of 550 °C to 800 °C on H_2 and CO concentration was studied with a calcination temperature of 400 °C, a holding time of 20 min, and NiO loading at 20 wt%. The dependence of H_2 and CO concentration on reaction temperature is depicted in Fig. 6, which conveys that the gas concentration increased with increasing reaction temperature when RS was pyrolyzed without a catalyst. Specifically, in the temperature range from 550 °C to 800 °C, H_2 and CO concentration experienced an upward trend from 3 vol% to 28 vol% and 16 vol% to 38 vol%, respectively. This may have been due to the decomposition of the long-chained compounds of the tars into relatively smaller components like light tar and gas at higher temperatures (see R1 below) (Ateş and Işıkdağ 2009).

Another noticeable parameter that improves the concentration of biomass pyrolysis syngas is the catalyst (Guo *et al.* 2018). As shown in Fig. 6, the concentration of H_2 and CO for RS pyrolysis with the NiO/FA catalyst was always remarkably higher than RS pyrolysis without the catalyst at the same experimental temperature. Compared with the results of RS pyrolysis without the catalyst, the H_2 and CO concentration when a NiO/FA catalyst was used increased 34 vol% and 16 vol% at 600 °C, respectively. The enhancement effect was more obvious than when other test temperatures were used, which indicated that

the NiO/FA catalyst exhibited the best performance at 600 °C. It has been reported that the high activity of Ni-based catalysts can be attributed to the fact that nickel is the main active component for activating the C-H and C-C bonds of tar compounds (Torres *et al.* 2007; Ahmed *et al.* 2009). In addition, Ni-based catalysts also activate the tar reforming reactions ((R2) through (R4)) (Guan *et al.* 2016), the water gas reaction (R5), and the water gas shift reaction (R6) (Wang *et al.* 2005). For the above reasons, the concentration of H_2 and CO greatly increased.

$$\text{Tars} \rightarrow C + C_xH_y + \text{Gases} \quad \text{(R1)}$$

$$C_xH_y + xH_2O \rightarrow xCO + (x + y/2)\,H_2 \quad \text{(R2)}$$

$$C_xH_y + 2xH_2O \rightarrow xCO_2 + (2x + y/2)\,H_2 \quad \text{(R3)}$$

$$C_xH_y + xCO_2 \rightarrow 2xCO_2 + (y/2)\,H_2 \quad \text{(R4)}$$

$$C + H_2O \leftrightarrow CO + H_2 \quad \text{(R5)}$$

$$CO + H_2O \leftrightarrow CO_2 + H_2 \quad \text{(R6)}$$

$$CO_2 + C \leftrightarrow CO \quad \text{(R7)}$$

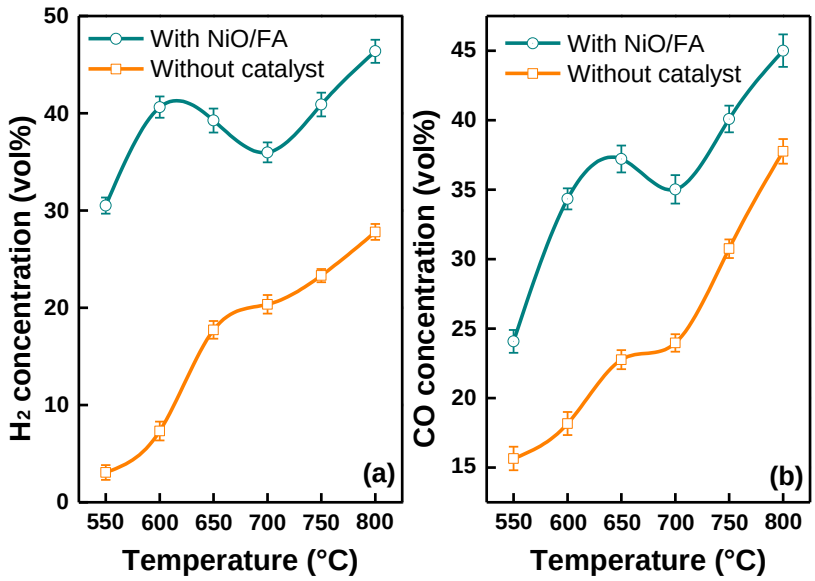

Fig. 6. Effect of reaction temperature on the concentration of (a) H_2 (vol%) and (b) CO (vol%)

High temperature and coke deposition are the main factors that deactivate Ni-based catalysts (Sehested 2006). Figure 6(a) shows that the concentration of H_2 decreased after 600 °C when the NiO/FA catalyst was used. The growth trend resumed after 700 °C, but the increasing amount of H_2 concentration, compared to the reaction without a catalyst at the same test temperature, evidently decreased with the rising temperature. Figure 6(b) exhibits a similar pattern. The concentration of CO decreased after 650 °C, which was slightly different from Fig. 6(a). It was concluded that the increase of reaction temperature degraded the performance of the catalyst. The coke deposition content of the catalyst at different reaction temperatures is described in Table 4, which showed that it first rose and then declined with increased temperature, and reached its maximum at 650 °C. This could

have been due to the secondary cracking of tar at around 650 °C (Watihan *et al.* 2018). The coke deposition rate was greater than the coke consumption rate, which increased the coke deposition content, resulting in a diminished metal active site reacting with the tar molecules, thereby reducing the activity of the catalyst (Hu, 2015). Consequently, the gas concentration decreased at around 650 °C. After 700 °C, due to the water gas reaction (R5) and the boudouard reaction (R7) (Elrub *et al.* 2008), the coke deposition rate accelerated, which led to the reduction of the coke content and the activation of the metal active site, which enhanced the catalytic reforming of tar (Hu *et al.* 2017). Therefore, the gas concentration rose again after 700 °C. The XRD pattern of the catalyst with different reaction temperatures is illustrated in Fig. 7. The NiO in the NiO/FA catalyst was first reduced to elementary Ni *via* the reductive atmosphere, including H_2 and CO, in crude pyrolysis gas, which then promoted the catalytic reforming of tar. Therefore, the characteristic peaks of NiO disappeared and were replaced by the characteristic peaks of elemental Ni after the reaction. Moreover, the characteristic diffraction peaks of Ni enhanced with increased temperature, which explained why the particle size of elemental Ni gradually increased. It was further speculated that the catalyst sintered at high temperature, which caused the concentrations of H_2 and CO to be reduced after 700 °C. Considering the best performance of the catalyst occurred at 600 °C, 600 °C was chosen as an appropriate reaction temperature in other experiments.

Table 4. Coke Deposition Content of NiO/FA with Different Reaction Temperatures

Temperature (°C)	600	650	700	800
C content (wt%)	2.12	2.57	1.03	0.94

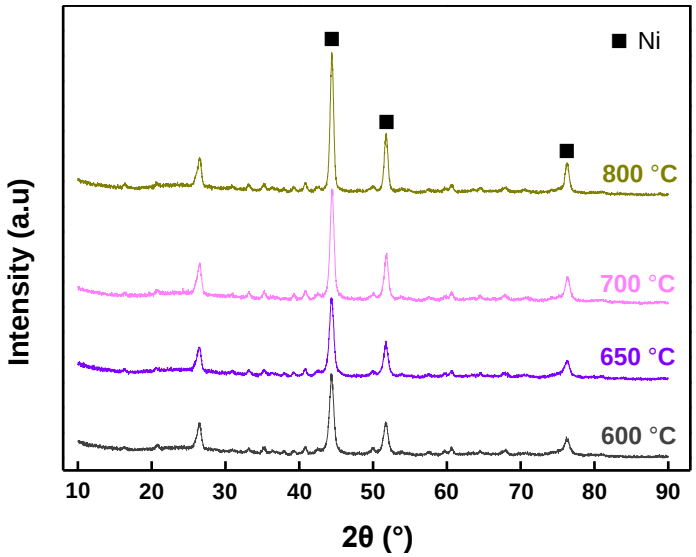

Fig. 7. The XRD pattern of the catalyst with different reaction temperatures

Effect of holding time

The effect of holding time from 5 min to 35 min on H_2 and CO concentration was investigated with calcination temperature, reaction temperature, and NiO loading at 400

°C, 600 °C, and 20 wt%, respectively. Figure 8 shows the gas concentration as a function of holding time. Both the H_2 and CO concentrations remained stable when the holding time was greater than 20 min but were reduced slightly below that point. Particularly, under the action of NiO/FA catalyst, H_2 and CO concentration increased from 35 vol% and 29 vol% at 5 min to 41 vol% and 34 vol% at 20 min, respectively. This result revealed that the maximum syngas concentration was reached at 20 min, even in the presence of the NiO/FA catalyst. Shi *et al.* (2018) showed that tar molecules, which can be catalytic, cracked and were almost decomposed after the holding time exceeded 20 min, and the syngas concentration was not remarkably improved with the increase of holding time. Longer holding times require more energy input. Therefore, a minimal but reasonable holding time, such as 20 min, was found to be favorable in this study.

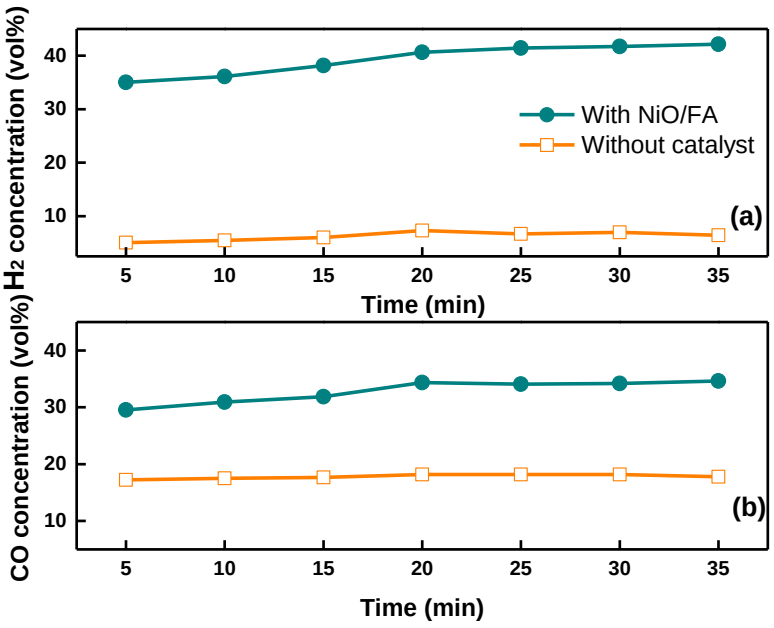

Fig. 8. Effect of holding time on the concentration of (a) H_2 (vol%) and (b) CO (vol%)

Effect of NiO loading

The effect of NiO loading on H_2 and CO concentration was studied with the NiO/FA catalyst at a calcination temperature of 400 °C, reaction temperature of 600 °C, and a 20 min holding time. The dependence of gas concentration on NiO loading is shown in Fig. 9. It is shown that with the increased loading of NiO from 0 wt% to 20 wt%, the H_2 concentration clearly increased from 7 vol% to 41 vol%, which suggests that Ni played a vital role in the promotion of H_2 generation. However, when NiO content further increased from 20 wt% to 30 wt%, the H_2 concentration was accompanied by a slight decrease. A similar observation was found in CO concentration, which shows that CO concentration peaked at 34 vol% when loaded with 20 wt% NiO. It can be seen from Fig. 3 (b),(d) and (e) that with the increase of loading, NiO agglomerated gradually on the FA surface. The XRD patterns of three different NiO loading catalysts are illustrated in Fig. 10. It can be observed that the NiO characteristic peaks became stronger and narrower with the increase of NiO content, indicating that the crystal size of NiO particles increased. This further reflected the occurrence of metal agglomeration. In addition, the BET surface area of the catalysts increased from 23.43 $m^2 \cdot g^{-1}$ of 10 wt% NiO loading to 36.24 $m^2 \cdot g^{-1}$ of 30 wt%, which was consistent with the FESEM results. These results indicated that excessive NiO

loading inhibited the increase of syngas concentration. Other researchers have drawn similar conclusions. Quan *et al.* (2017) suggested that the high loading of NiO reduced the dispersion of metal and increased the aggregation of active sites, thus causing a lower efficiency. Chen *et al.* (2017) explained that the overload of nickel resulted in a reduction of available catalytic surface area and subsequently the performance of the catalyst declined.

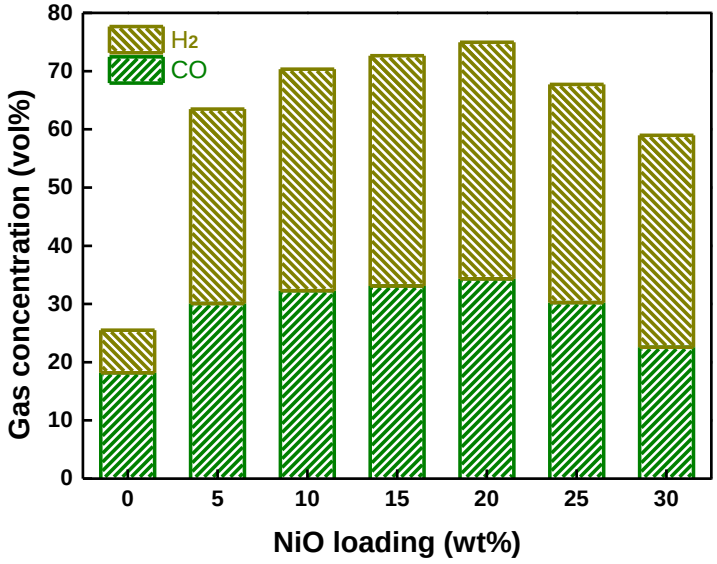

Fig. 9. Effect of NiO loading on the concentration of H_2 (vol%) and CO (vol%)

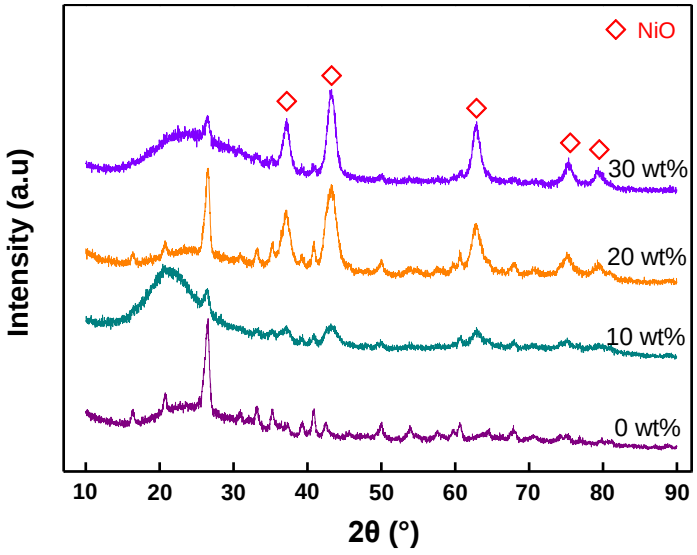

Fig. 10. XRD patterns of NiO/FA catalysts with different NiO loading

It was noteworthy that the concentration of H_2 and CO was equivalent to RS pyrolysis alone when the FA was used as catalyst. This result revealed that the FA of this study did not have the catalytic capacity. This was slightly different from the results obtained by Loy *et al.* (2018b), who used fly ash as catalyst for the catalytic pyrolysis of rice husk to obtain an H_2 increase of 8.4 vol%. The analysis suggested that it may have been due to the difference in fly ash composition. In Loy *et al.*'s (2018b) study, the content

of Fe_2O_3 and CaO in fly ash were 21.2 wt% and 15.0 wt%, respectively, compared with only 3.9 wt% and 5.8 wt% in this experiment, respectively. It is well known that Fe_2O_3 and CaO can play a catalytic role in the pyrolysis of biomass, thus increasing the syngas concentration. Xu *et al.* (2012) found that the H_2 concentration improved approximately 25 vol% after using the Fe_2O_3/γ-Al_2O_3 catalyst in the study of hydrogen production from rice husk catalytic cracking. Li *et al.* (2016) investigated the effect of CaO on hydrogen production from pyrolysis of corn straw and found that the H_2 concentration increased approximately 28 vol% due to the presence of CaO. Furthermore, different experimental process conditions can also lead to differences in this result.

regeneration of the used catalyst

Recycling and reuse of the used catalyst in the catalytic pyrolysis process were investigated by an oxidative thermal treatment. The used catalyst was heated from 20 °C to 600 °C with a rate of 10 °C /min in an air atmosphere and maintained at 600 °C for 2 h. The performance of regenerated catalyst was evaluated and shown in Fig. 11. It can be observed that compared with the results of fresh catalyst, the catalytic performance of regenerated catalyst for syngas production decreased slightly. But the syngas concentration was still above 60 vol%. In order to achieve the purpose of large-scale industrial application, in the future work, promoters such as rare earth metals can be added to further improve and stabilize the performance of the NiO/FA catalyst in syngas production.

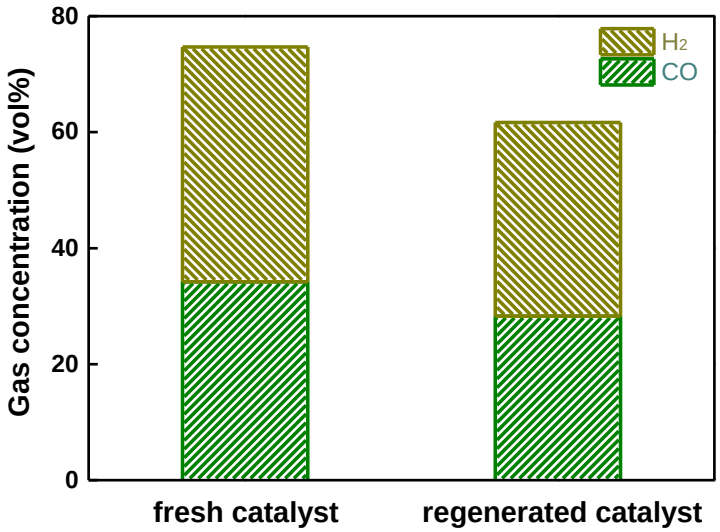

Fig. 11. Comparison of catalytic performance between fresh catalyst and regenerated catalyst

CONCLUSIONS

1. The active component metallic nickel was successfully loaded onto the fly ash surface in the form of nickel oxide *via* homogeneous precipitation, and NiO was well dispersed on the surface of fly ash by a filament-like coating.
2. The optimum performance of the NiO/FA catalyst for the production of H_2 and CO was obtained at a calcination temperature of 400 °C, reaction temperature of 600 °C, holding time of 20 min, and NiO loading of 20 wt%.

3. With increased calcination temperature from 400 °C to 700 °C, the concentration of syngas gradually decreased from 75 vol% to 58 vol%, and the particle size of NiO in the catalyst gradually increased.
4. In the presence of the NiO/FA catalyst, the concentration of syngas peaked at the reaction temperature of 600 °C and slightly decreased after that. Although the increasing trend resumed after 700 °C, the increasing amount was remarkably reduced.
5. Under the action of the NiO/FA catalyst, H_2 and CO concentration increased from 35 vol% and 29 vol% at 5 min to 41 vol% and 34 vol% at 20 min, respectively, and then remained stable.
6. Excessive NiO loading inhibited the increase of syngas concentration. When loaded with 20 wt%, the NiO/FA catalyst had the best performance of 41 vol% H_2 and 34 vol% CO.

ACKNOWLEDGMENTS

The authors are grateful for the support of the Technical Innovation Major Project of Hubei Province, Grant No. 2017ABA155 and the Central Committee Guides Local Science and Technology Development Special Project of Hubei Province, Grant No. 2018ZYYD062.

REFERENCES CITED

Ahmed, S., Aitani, A., Rahman, F., Al-Dawood, A., and Al-Muhaish, F. (2009). "Decomposition of hydrocarbons to hydrogen and carbon," *Appl. Catal. A- Gen.* 359(1-2), 1-24. DOI: 10.1016/j.apcata.2009.02.038

Akubo, K., Nahil, M. A., and Williams, P. T. (2018). "Pyrolysis-catalytic steam reforming of agricultural biomass wastes and biomass components for production of hydrogen/syngas," *J. Energy. Inst.* DOI: 10.1016/j.joei.2018.10.013

Ateş, F., and Işıkdağ, M. A. (2009). "Influence of temperature and alumina catalyst on pyrolysis of corncob," *Fuel* 88(10), 1991-1997. DOI: 10.1016/j.fuel.2009.03.008

Balasundram, V., Ibrahim, N., Kasmani, R. M., Hamid, M. K. A., Isha, R., Hasbullah, H., and Ali, R. R. (2018). "Thermogravimetric catalytic pyrolysis and kinetic studies of coconut copra and rice husk for possible maximum production of pyrolysis oil," *J. Clean. Prod.* 167, 218-228. DOI: 10.1016/j.jclepro.2017.08.173

Bo, L. L., Wang, X. C., Wang, M. G., and Zhou, L. H. (2008). "Characteristics of carbon-supported metal catalyst prepared by microwave method*," Journal of Xi'an University of Architecture & Technology* 40(4), 532-537. DOI: 10.15986/j.1006-7930.2008.04.005

Buchireddy, P. R., Bricka, R. M., Rodriguez, J., and Holmes, W. (2010). "Biomass gasification: Catalytic removal of tars over zeolites and nickel supported zeolites," *Energ. Fuel.* 24(4), 2707-2715. DOI: 10.1021/ef901529d

Chang, A. C.-C., Chang, L.-S., Tsai, C.-Y., and Chan, Y.-C. (2014). "Steam reforming of gasification-derived tar for syngas production," *Int. J. Hydrogen Energ.* 39(33), 19376-19381. DOI: 10.1016/j.ijhydene.2014.07.133

Chen, G. Y., Li, J., Liu, C., Yan, B. B., Cheng, Z. J., Ma, W. C., Yao, J. G., and Zhang, H. (2017). "Low-temperature catalytic cracking of biomass gasification tar over Ni/HZSM-5," *Waste Biomass Valori.* 10(4), 1013-1020. DOI: 10.1007/s12649-017-0107-7

Choudhary, V. R., and Mamman, A. S. (2000). "Energy efficient conversion of methane to syngas over NiO–MgO solid solution," *Appl. Energ.* 66(2), 161-175. DOI: 10.1016/S0306-2619(99)00039-2

Courson, C., Udron, L., Świerczyński, D., Petit, C., and Kiennemann, A. (2002). "Hydrogen production from biomass gasification on nickel catalysts: Tests for dry reforming of methane," *Catal. Today* 76(1), 75-86. DOI: 10.1016/S0920-5861(02)00202-X

Duman, G., Watanabe, T., Uddin, M. A., and Yanik, J. (2014). "Steam gasification of safflower seed cake and catalytic tar decomposition over ceria modified iron oxide catalysts," *Fuel Process. Technol.* 126, 276-283. DOI: 10.1016/j.fuproc.2014.04.035

Elrub, Z. A., Bramer, E. A., and Brem, G. (2008). "Experimental comparison of biomass chars with other catalysts for tar reduction," *Fuel* 87(10-11), 2243-2252. DOI: 10.1016/j.fuel.2008.01.004

Field, C. B., Campbell, J. E., and Lobell, D. B. (2008). "Biomass energy: The scale of the potential resource," *Trends Ecol. Evol.* 23(2), 65-72. DOI: 10.1016/j.tree.2007.12.001

Furusawa, T., and Tsutsumi, A. (2005). "Comparison of Co/MgO and Ni/MgO catalysts for the steam reforming of naphthalene as a model compound of tar derived from biomass gasification," *Appl. Catal. A- Gen.* 278(2), 207-212. DOI: 10.1016/j.apcata.2004.09.035

Gao, N. B., Han, Y., Quan, C., and Wu, C. F. (2017). "Promoting hydrogen-rich syngas production from catalytic reforming of biomass pyrolysis oil on nanosized nickel-ceramic catalysts," *Appl. Therm. Eng.* 125, 297-305. DOI: 10.1016/j.applthermaleng.2017.07.028

Garbarino, G., Wang, C., Valsamakis, I., Chitsazan, S., Riani, P., Finocchio, E., Flytzani-Stephanopoulos, M., and Busca, G. (2015). "A study of Ni/Al_2O_3 and $Ni-La/Al_2O_3$ catalysts for the steam reforming of ethanol and phenol," *Appl. Catal. B– Environ.* 174-175, 21-34. DOI: 10.1016/j.apcatb.2015.02.024

GB/T 28731 (2012). "Proximate analysis of solid biofuels," Standardization Administration of China, Beijing, China.

Guan, G. Q., Kaewpanha, M., Hao, X. G., and Abudula, A. (2016). "Catalytic steam reforming of biomass tar: Prospects and challenges," *Renew. Sust. Energ. Rev.* 58, 450-461. DOI: 10.1016/j.rser.2015.12.316

Guo, F. Q., Li, X. L., Liu, Y., Peng, K. Y., Guo, C. L., and Rao, Z. H. (2018). "Catalytic cracking of biomass pyrolysis tar over char-supported catalysts," *Energy Convers. Manage.* 167, 81-90. DOI: 10.1016/j.enconman.2018.04.094

He, M. Y., Xiao, B., Hu, Z. Q., Liu, S. M., Guo, X. J., and Luo, S. Y. (2009). "Syngas production from catalytic gasification of waste polyethylene: Influence of temperature on gas yield and composition," *Int. J. Hydrogen Energ.* 34(3), 1342-1348. DOI: 10.1016/j.ijhydene.2008.12.023

Hu, M. (2015). *Preparation and Mechanism for Char Supported Fe-Ni Catalysts on Biomass Catalytic Pyrolysis*, Ph.D. Dissertation, Huazhong University of Science and Technology, Wuhan, China.

Hu, M., Laghari, M., Cui, B., Xiao, B., and Guo, D. (2017). "Catalytic cracking of biomass tar over char supported nickel catalyst," *Energy* 145, 228-237. DOI: 10.1016/j.energy.2017.12.096

Hu, M., Wang, X., Chen, J., Yang, P., Liu, G. X., Xiao, B., and Guo, D. B. (2017). "Kinetic study and syngas production from pyrolysis of forestry waste," *Energ. Convers. Manage.* 135, 453-462. DOI: 10.1016/j.enconman.2016.12.086

Li, B., Han, X., Chen, Y. L., Wei, L. Y., Yang, H. P., and Chen, H. P. (2016). "Effects of calcium-based absorbents on hydrogen production of corn stalk pyrolysis-gasification," *Renewable Energy Resources* 35(4), 502-507. DOI: 10.6041/j.issn.1000-1298.2016.08.027

Li, C. S., Hirabayashi, D., and Suzuki, K. (2010). "Steam reforming of biomass tar producing H_2-rich gases over Ni/MgO_x /CaO_{1-x} catalyst," *Bioresource Technol.* 101(1), 97-100. DOI: 10.1016/j.biortech.2009.03.043

Li, D. L., Ishikawa, C., Koike, M., Wang, L., Nakagawa, Y., and Tomishige, K. (2013). "Production of renewable hydrogen by steam reforming of tar from biomass pyrolysis over supported Co catalysts," *Int. J. Hydrogen Energ.* 38(9), 3572-3581. DOI: 10.1016/j.ijhydene.2013.01.057

Li, J. F., Xiao, B., Yang, J. K., and Jia, L. (2006). "Preparation of catalyst support for biomass pyrolysis from industrial waste and its properties," *Environ. Eng.* 24(6), 56-58. DOI: 10.13205/j.hjgc.2006.06.017

Liu, X. J., Wang, H., and Liu, L. L. (2018). "Development and utilization of fly ash resources," *Inorg. Chem. Ind.* 354(05), 16-18.

Loy, A. C. M., Yusup, S., Chin, B. L. F., Gan, D. K. W., Shahbaz, M., Acda. M. N., Unrean, P., and Rianawati. E. (2018a). "Comparative study of in-situ catalytic pyrolysis of rice husk for syngas production: Kinetics modelling and product gas analysis," *J. Clean. Prod.* 197, 1231-1243. DOI: 10.1016/j.jclepro.2018.06.245

Loy, A. C. M., Yusup, S., Lam, M. K., Chin, B. L. F., Shahbaz, M., Yamamoto, A., and Acda, M. N. (2018b). "The effect of industrial waste coal bottom ash as catalyst in catalytic pyrolysis of rice husk for syngas production," *Energ. Convers. Manage.* 165, 541-554. DOI: 10.1016/j.enconman.2018.03.063

Michel, R., Lamacz, A., Krzton, A., Djéga-Mariadassou, G., Burg, P., Courson, C., and Gruber, R. (2013). "Steam reforming of α-methylnaphthalene as a model tar compound over olivine and olivine supported nickel," *Fuel* 109, 653-660. DOI: 10.1016/j.fuel.2013.03.017

Nagrockiene, D., and Rutkauskas, A. (2019). "The effect of fly ash additive on the resistance of concrete to alkali silica reaction," *Constr. Build. Mater.* 201, 599-609. DOI: 10.1016/j.conbuildmat.2018.12.225

National Bureau of Statistics of China. (2017). "Output of major crop products," (http://www.stats.gov.cn), Accessed 30 December 2018.

Panwar, N. L., Kaushik, S. C., and Kothari, S. (2011). "Role of renewable energy sources in environmental protection: A review," *Renew. Sust. Energ. Rev.* 15(3), 1513-1524. DOI: 10.1016/j.rser.2010.11.037

Quan, C., Gao, N. B., and Wu, C. F. (2017). "Utilization of NiO/porous ceramic monolithic catalyst for upgrading biomass fuel gas," *J. Energy Inst.* 91(3), 1-8. DOI: 10.1016/j.joei.2017.02.008

Roh, H. S., Eum, I. H., Jeong, D. W., Yi, B. E., Na, J. G., Ko, C. H. (2011). "The effect of calcination temperature on the performance of Ni/MgO–Al_2O_3 catalysts for

decarboxylation of oleic acid," *Catal. Today* 164(1), 457-460. DOI: 10.1016/j.cattod.2010.10.048

Sehested, J. (2006). "Four challenges for nickel steam-reforming catalysts," *Catal. Today* 111(1-2), 103-110. DOI: 10.1016/j.cattod.2005.10.002

Shao, S., Zhang, H., Xiao, R., Li, X., and Cai, Y. (2018). "Controlled regeneration of ZSM-5 catalysts in the combined oxygen and steam atmosphere used for catalytic pyrolysis of biomass-derivates," *Energy Convers. Manage.* 155, 175-181. DOI: 10.1016/j.enconman.2017.10.062

Shi, X. W., Xin, X., Liu, Z., Lu, Y., Li, H. Y., Cheng, Q. P., and Li, J. F. (2018). "Preparation and characterization of Ni/TPC catalyst and applied in straw pyrolysis gas reforming," *J. Fuel. Chem. Technol.* 46(6), 659-665. DOI: 10.1016/S1872-5813(18)30028-8

Sun, Y., Liu, L., Wang, Q., Yang, X., and Tu, X. (2016). "Pyrolysis products from industrial waste biomass based on a neural network model," *J. Anal. Appl. Pyrol.* 120, 94-102. DOI: 10.1016/j.jaap.2016.04.013

Suzuki, T., Ohme, H., and Watanabe, Y. (1992). "Alkali metal catalyzed carbon dioxide gasification of carbon," *Energ. Fuel* 6(4), 343-351. DOI: 10.1021/ef00034a003

Świerczyński, D., Libs, S., Courson, C., and Kiennemann, A. (2007). "Steam reforming of tar from a biomass gasification process over Ni/olivine catalyst using toluene as a model compound," *Appl. Catal. B – Environ.* 74(3-4), 211-222. DOI: 10.1016/j.apcatb.2007.01.017

Torres, W., Pansare, S. S., and Goodwin, J. G. (2007). "Hot gas removal of tars, ammonia, and hydrogen sulfide from biomass gasification gas," *Catal. Rev.* 49(4), 407-456. DOI: 10.1080/01614940701375134

Valle, B., Aramburu, B., Remiro, A., Bilbao, J., and Gayubo, A. G. (2014). "Effect of calcination/reduction conditions of Ni/La_2O_3-αAl_2O_3 catalyst on its activity and stability for hydrogen production by steam reforming of raw bio-oil/ethanol," *Appl. Catal. B – Environ.* 147, 402-410. DOI: 10.1016/j.apcatb.2013.09.022

Wang, T. J., Chang, J., Wu, C. Z., Fu, Y., and Chen, Y. (2005). "The steam reforming of naphthalene over a nickel–dolomite cracking catalyst," *Biomass Bioenerg.* 28(5), 508-514. DOI: 10.1016/j.biombioe.2004.11.006

Wang, G. Y., Xu, S. P., Wang, C., Zhang, J. J., and Fang, Z. J. (2017). "Desulfurization and tar reforming of biogenous syngas over Ni/olivine in a decoupled dual loop gasifier," *Int. J. Hydrogen Energ.* 42(23), 15471-15478. DOI: 10.1016/j.ijhydene.2017.05.041

Wang, Y. C., and Zhao, J. P. (2019). "Facile preparation of slag or fly ash geopolymer composite coatings with flame resistance," *Constr. Build. Mater.* 203, 655-661. DOI: 10.1016/j.conbuildmat.2019.01.097

Watihan, B., Tursun, Y., Talifu, D., and Abulizi, A. (2018). "Influence of the nickel loaded olivine catalyst on the pyrolysis of cotton stalk," *Renew. Energ. Res.* 36(7), 969-976. DOI: 10.13941/j.cnki.21-1469/tk.2018.07.004

Xu, X., Jiang, E. C., Wang, M. F., Li, B. S., and Zhou, L. (2012). "Hydrogen production by catalytic cracking of rice husk over Fe2O3/γ-Al2O3 catalyst," *Renew. Energ.* 41, 23-28. DOI: 10.1016/j.renene.2011.09.004

Xue, Y., Johnston, P., and Bai, X. (2017). "Effect of catalyst contact mode and gas atmosphere during catalytic pyrolysis of waste plastics," *Energy Convers. Manage.* 142, 441-451. DOI: 10.1016/j.enconman.2017.03.071

Yang, S. X., Zhang, X. D., Chen, L., Sun, L. Z., Xie, X. P., and Zhao, B. F. (2017). "Production of syngas from pyrolysis of biomass using Fe/CaO catalysts: Effect of operating conditions on the process," *J. Anal. Appl. Pyrolysis* 125. DOI: 10.1016/j.jaap.2017.05.007

Yu, Q.-Z., Brage, C., Nordgreen, T., and Sjöström, K. (2009). "Effects of Chinese dolomites on tar cracking in gasification of birch," *Fuel* 88(10), 1922-1926. DOI: 10.1016/j.fuel.2009.04.020

Zhang, Z. K., Liu, L., Shen, B. X., and Wu, C. F. (2018). "Preparation, modification and development of Ni-based catalysts for catalytic reforming of tar produced from biomass gasification," *Renew. Sust. Energ. Rev.* 94, 1086-1109. DOI: 10.1016/j.rser.2018.07.010

Article submitted: April 17, 2019; Peer review completed: June 23, 2019; Revised version received and accepted: July 5, 2019; Published: July 12, 2019.
DOI: 10.15376/biores.14.3.6983-7000